Surface effects of bottom-generated turbulence in a shallow tidal sea

W. A. M. Nimmo Smith, S. A. Thorpe & A. Graham

School of Ocean and Earth Science, Southampton Oceanography Centre, European Way, Southampton SO14 3ZH, UK

Turbulence in shelf seas strongly affects the spread of pollution (such as oil spills[1]) as well as the distribution of sediment[2] and phytoplankton blooms[3]. Turbulence is known to be generated intermittently close to the sea bed[4], but little is known of its evolution through the water column, or to what extent it affects the surface. Here we present observations of the surface effects of bottom-generated turbulence in a tidally influenced and well mixed region of the North Sea, as derived from acoustic and visual images. Although the sea bed in the area is flat, we find that at any one time, 20–30% of the water surface is affected by boils—circular regions of local upwelling—of diameter 0.9±0.2 times the water depth. The signature of individual boils persists for at least 7 minutes and, in accordance with laboratory[5,6] and numerical[7] studies, shows the appearance of eddies. The boils contribute to the replacement of surface waters from depth in unstratified waters, and may therefore enhance the fluxes of gases between atmosphere and ocean.

There are no reported observations of the surface signature of boils in well mixed, open sea. It is, however, clear from dynamical measurements made using current meters that tidal flows generate turbulence through the action of shear stress at the sea bed in much the same manner as in channels in laboratory experiments[4,8]. Fluid is intermittently ejected away from the bottom in turbulent bursts that may reach vertical speeds of 25% of the forcing current[4]. Numerical[7] and laboratory[5,6] studies show that the upward-moving water produces a boil as it impinges on the water surface.

Upward-pointing side-scan sonar has been used to observe a wide variety of processes in the upper ocean[9–13]. In experiments designed to study the processes leading to dispersion of an oil plume in the tidally well mixed—and consequently unstratified[14]—southern North Sea, a two-beam side-scan sonar system was mounted on a frame set on the sea bed at a depth of 45 m. The sonars operate at 80 kHz and 90 kHz, are set at 90° apart in the horizontal, and produce vertical fan-like beams with axes aligned upwards, 20° from the horizontal[15]. The site is 56 km from the shore and the local sea bed is flat, with no sand banks or other notable bed forms. The principal acoustic scatterers are bubbles, of typical diameter 20–200 μm, produced in clouds by wind waves as they break[16]. The clouds are detectable to ranges of ~150 m along the sea surface from the sonar, bubbles accumulating in regions of surface convergence and downwelling[17,18]. Oil reduces wave breaking and acoustic scatter from the sea surface[10]. Acoustic observations were made, however, at least 0.5 km from the oil plume, and in a variety of wind speeds from near calm to 14 m s^{-1} and in tidal currents reaching 1 m s^{-1}.

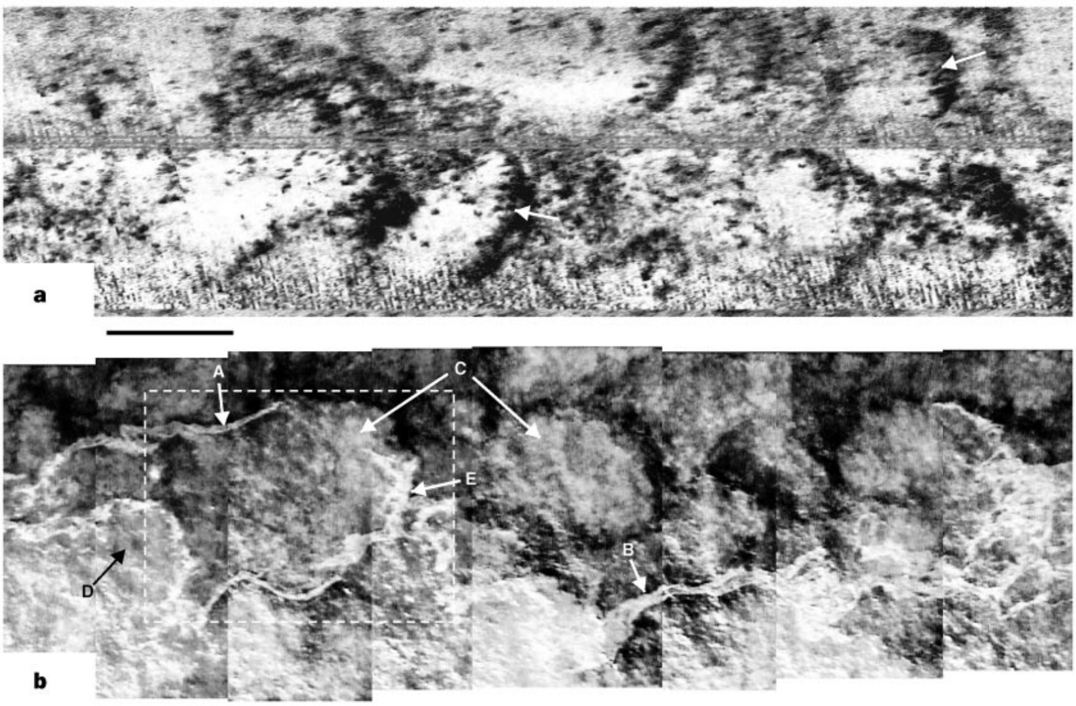

Figure 1 Sonar and video images of boils at the sea surface. The scale is the same in both images (and along both axes), and the tidal current is from right to left; scale bar, 50 m. **a**, Sonograph from a side-scan sonar beam directed across the tidal current showing crescent-shaped dark patterns (as, for example, shown by arrows) from which sound scattering is intense. The mean flow is 0.98±0.03 m s^{-1} at 17 m depth and 0.75±0.02 m s^{-1} at 33 m depth measured by moored vector-averaging current meters. The tidal current changed by less than 0.1 m s^{-1} h^{-1}. The wind 10 m above the sea surface is 6.4 ± 0.4 m s^{-1}, headed 43 ± 10° left of the current. The image is derived over a 10-min period, 3.5 h after slack water, and as the features shown are being advected through the sonar beam, the timescale has been accordingly converted into distance using their advective speed, 0.89 m s^{-1}, as measured by the sonar directed into the current. The band ~65 m from the lower edge results from electrical interference. The faint pattern of near-vertical bands at the lower edge results from reflections from surface waves, of period 3.4 s. **b**, Composite image from video of the oil plume being advected from right to left. Oil appears white or nearly white; in this location, ~1.6 km from the source of the plume, the oil has a filamentary structure (for example, as shown at 'A' and 'B'). Sun-glint is affecting the image along the lower edge, and bright speckles in the centre are caused by sunlight reflecting from surface waves. Lighter blobs show patches of particulate material surrounded by darker regions of clearer water (for example, at positions 'C'). Feature 'D' and the development of the plume within the dashed box are discussed in Fig. 2 legend; oil at 'E' has dispersed laterally around a boil (that is, normal to the mean direction of plume advection).

In low tidal flows and winds exceeding $\sim 4 \text{ m s}^{-1}$, the dominant features observed in the sonograph images of the sea surface are the well-known[9,11,15,18] linear bands of bubble clouds aligned close to the wind direction in the convergence zones created between neighbouring Langmuir cells. In stronger tidal currents, however, the linear bands were found to be replaced by crescent-shaped features (Fig. 1a). They have a mean diameter of 42 ± 10 m ($\pm$ implies one standard deviation) or $(0.93 \pm 0.22)H$, where H is the water depth. The crescents are almost semicircular and are advected with the current. The mean number of features with centres passing through unit length of the sonar beam in unit time is $N = (9.4 \pm 3.3) \times 10^{-5} \text{ m}^{-1} \text{ s}^{-1}$. The sonar beam pointing into the current shows the features to be drifting down-current through the beam at speeds of $0.89 \pm 0.09 \text{ m s}^{-1}$. Such speeds are greater than that of the tidal current at 33 m depth ($0.75 \pm 0.02 \text{ m s}^{-1}$) but less than that at 17 m depth($0.98 \pm 0.03 \text{ m s}^{-1}$); they are also less than the speeds of isolated bubble clouds ($1.29 \pm 0.08 \text{ m s}^{-1}$) seen in the sonar image, which are characteristic of the wind drift and tidal current in the upper 1 m of the water column[9,13,16].

Video images of the oil plume and of the surrounding water surface up to 2 km downstream of a fixed, steady source were obtained at 5-min intervals by an overflying aircraft, 1 h before the sonograph shown in Fig. 1a was obtained. Figure 1b is a composite image of frames 'grabbed' from the video. It shows the plume, which has become filamentary, and, in particular, the appearance of local regions where the oil is abruptly dispersed normal to the direction in which it is being advected (for example, within the dashed box). Oil accumulates in a convergence zone at the upstream edge of these roughly circular regions, and spreads to either side (see also Fig. 2a). The mean diameter of these regions is 47 ± 14 m or $(1.04 \pm 0.31)H$, and they cover a proportion, $p \approx 0.2$, of the water surface. Features tracked in the oil plume through a sequence of video images decay or are engulfed in new, but similar, features in a time, $\tau = 410 \pm 140$ s, given as a lower bound because of the limited time-span of the images. Figure 1b also shows patches of discoloured water of lighter shading than their surroundings (for example, arrowed 'C'). Their mean diameter is 65 ± 15 m or $(1.44 \pm 0.33)H$, and they cover $p \approx 0.3$ of the water surface. The number of such features per unit area is therefore $0.3/[(\pi/4)65^2] = 9.0 \times 10^{-5} \text{ m}^{-2}$. The discoloration seems to result from the presence of particulate matter, probably sediment, originating from—and pointing to—a local source at the sea bed. The evolution of these features is also seen in the Compact Airborne Spectrographic Imager (CASI) images of the break-up of an oil patch (Fig. 3).

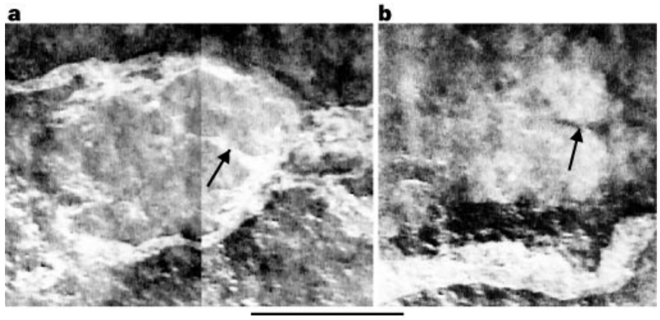

Figure 2 Video images showing details of boils. The tidal current and scales are as for Fig. 1. **a**, The break-up of the oil plume. This is the region within the dashed box at the left of Fig. 1b, but 5 min earlier: abrupt spreading of oil normal to the direction of its advection is evident about a roughly circular sediment patch. By the time of Fig. 1b, the plume at the lower edge of the patch has been distorted by the growth of a new boil, marked therein as 'D'. **b**, A sediment patch lying outside the oil plume (part of which is visible as a white band running across the figure at the bottom). The image shows a characteristic feature, a filament (arrowed), connecting to the upstream side. A similar feature is arrowed in the oil pattern in **a**.

The acoustic and visually observed features have the characteristics of boils often seen in fast-flowing shallow rivers and narrow channels[19,20]. Boils are produced as upwelling water interacts with, and spreads radially on, the surface[21,22]. They are often visible in low winds because of their effect in steepening short surface gravity waves[20]. In laboratory experiments in a channel[5,6], dye released near the bottom shows that the boils originate in intermittent ejections from the shear-stress-generated turbulent boundary layer overlying the channel bed. They occur when the upward-moving ejected water impinges on the water surface[5,6]. Eddies evolve at the edges, and downstream, of the boils[6]. This is consistent with our observations; about 44% of the sediment patches observed in the video images (covering $\sim 0.5 \text{ km}^2$) are divided in two by filaments, 8.6 ± 2.4 m in width, roughly aligned with the current (Fig. 2b), suggesting that they consist of pairs of counter-rotating eddies producing an upstream flow along the axis of the features and convergence at their upstream edge. The characteristics of the surface eddies observed in the laboratory, such as separation and size, are found to depend both on outer variables (the free-flow speed, U, and water depth, H) and on inner variables (the friction

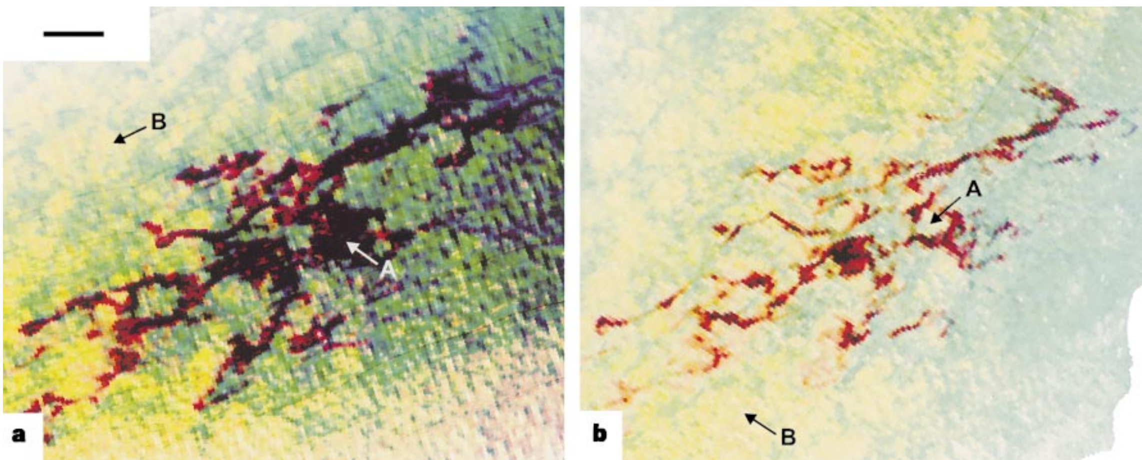

Figure 3 CASI false-colour images of an oil patch (in red). The two images are of the same area of sea surface; **a** was taken 5 min before **b**. Scale bar, 100 m in both images. The oil has dispersed from a patch in the southern North Sea over a period of 4 tides (2 days) in an area of uniform depth, 45 m. The colour scale is different between the images, and **a** has been affected by cloud shadow. Oil thicker than 250 μm is imaged as red to black, while yellow and green result from ambient sea water and oil thinner than 5 μm. A roughly circular pale blob, of diameter 50 m, is formed within feature 'A' in the oil in the time between the two images. The yellow blobs (for example, at 'B') are clouds of particulates (see also Figs 1b ('C') and 2b). North is to the top. The wind speed 10 m above the sea is 6.3 m s^{-1} from 340°, and the current at 5 m depth is 0.99 m s^{-1} heading to 189°.

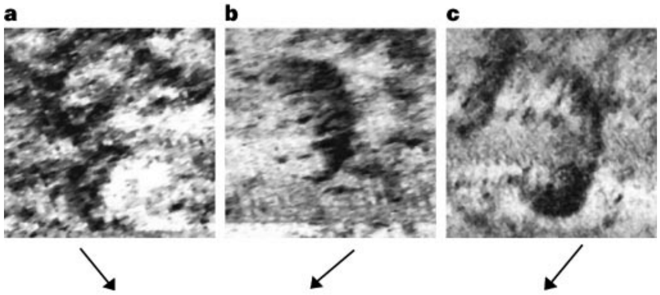

Figure 4 Sonograph images of strongly scattering features (shown as dark) in winds of different directions. The features are represented using the same frozen-field technique described in Fig. 1 legend. In each image, the tidal current is from right to left and the wind direction is shown by an arrow. Each image shows an area 60 m square. The mean current and 10-m wind speed are, respectively, **a**, 0.60 m s^{-1} (at 19 m depth), 3.0 m s^{-1}; **b**, 0.98 m s^{-1} (at 17 m depth), 6.3 m s^{-1}; **c**, 0.80 m s^{-1} (at 15 m depth), 7.1 m s^{-1}.

velocity at the bed, and the kinematic viscosity, ν). The diameter of the laboratory eddies decreases with increasing Reynolds number, Re $= UH/\nu$, being about $3H$ at Re $= 8.8\times10^3$, and greater than the size, about H, of eddies marked by sediment in the North Sea. The laboratory Reynolds number is, however, relatively small, ranging from 4.0×10^3 to 8.8×10^3, whereas Re is about 4.5×10^7 in the North Sea. Whilst the relatively smaller size of the sediment patches may be accounted for by the sinking of sediment (probably faster than 5×10^{-3} m s^{-1}, the settling speed of particulates in the region[2]), the observation that the laboratory scaling depends on inner variables suggests that the differences in scale may be simply a consequence of the difference in Re.

The boils travel at a velocity different from the combined tidal and wind-drift surface current. As shown by the sonograph images of features found given different relative orientations between wind and tidal current (Fig. 4), in ~90% of cases the acoustic scattering is greatest on the side from which the relative wind-drift comes. The boils are therefore visible in the sonar images because the downwelling, or 'downdrafts'[22], at their upwind boundary results in the local accumulation of bubbles[17,18] and wave steepening[20] or even breaking with bubble production, these effects enhancing the scattering of sound there. The surface expression of the boils lags the increasing tidal flow by 100–150 min; this is consistent with other sonar data[15], observations of suspended sediment concentration[2], and measurements and models of the kinetic energy of developing turbulence[23,24]. In consequence, boils are only observed at the surface for ~70% of the tidal cycle.

Figures 1b, 2a and 3 demonstrate the dispersive effects of the boils on floating material. Neglecting wind, the horizontal dispersion coefficient normal to a steady tidal current over a smooth bottom is $K = \beta UH$, where β is a constant[25]. A rough estimate for β can be found from the images. Boils produce a lateral spread of floating particles over scales of order H at times corresponding to those separating the arrival of boils at a given position following the flow. If f is the number of boils produced per unit area per unit time, and τ is their average 'lifetime', then the number of boils reaching the surface per unit area is $f\tau$. If $(1-\epsilon)$ is the fraction of area in which boils overlap and they are advected at speed U, the number of separate boils with centres passing a unit line normal to the flow in unit time is $N = f\epsilon\tau U$. If A is the area of a single boil then $p = f\tau A\epsilon = AN/U = 0.14\pm0.07$ from sonar data (compared to the observed $p \approx 0.2$). The surface area fraction covered per unit time is $fA\epsilon$ and the average time for an area to be covered is $T = (fA\epsilon)^{-1}$, the mean time between boils affecting a given area moving with the mean flow. The dispersion coefficient is $\sim H^2/T$, or $ANH^2/\tau U$, so that β $(=ANH/\tau U^2)$ ranges from 6.4×10^{-3} to 3.9×10^{-2}, using the sonar data and the probable underestimate of τ based on the oil plume. This spans the values, $\beta = (1.0\pm0.4)\times10^{-2}$, found in smooth-bottomed laboratory channels[26], though the dependence on Re is uncertain.

The images capture the generation of tidal boils and eddies over a level sea bed, showing that they are likely to be of common occurrence in tidal shelf-seas. They also provide insight into the vertical transport of water, sediment and algae on the shelf, at the larger scales that develop following ejections in turbulent bursts from close to the sea bed. The boils impose a patchy structure in, for example, the colour of the water surface (see Figs 1b, 2 and 3), which may bias the measured average values of sea-surface parameters detected by satellite or other 'remote' sensors. The images illustrate how boils disperse oil patches or plumes. Turbulence generated by the shear stress of tidal flow on the sea bed is evidently an important process of short-term dispersion in tidally mixed shelf seas, at least in wind speeds less than about $15U$ (ref. 27), at scales smaller than the Rossby radius (when rotation becomes significant) and until bathymetry becomes important[28]; in stronger winds, dispersion resulting from Langmuir circulation[12] may dominate. The appearance of the circles in the oil films (Fig. 3) demonstrates that boils help to replenish surface waters, a process important in gas exchange[16,29]. Such boils will be absent at the surface of density-stratified seas, where the thermocline separates the surface and the deep water, preventing bursts and ejections generated in the benthic boundary layer from reaching the surface. The intensity of near-surface turbulence and the rate of air–sea gas exchange in deep stratified oceanic waters may in consequence be lower than in well mixed tidal seas. □

Received 21 December 1998; accepted 21 May 1999.

1. Murray, S. P. Turbulent diffusion of oil in the ocean. *Limnol. Oceanogr.* **17,** 651–660 (1972).
2. Jago, C. F. & Jones, S. E. Observation and modelling of the dynamics of benthic fluff resuspended from a sandy bed in the southern North Sea. *Continent. Shelf Res.* **18,** 1255–1282 (1998).
3. Tett, P. B. *et al.* Biological consequences of tidal stirring gradients in the North Sea. *Phil. Trans. R. Soc. Lond. A* **343,** 493–508 (1993).
4. Heathershaw, A. D. "Bursting" phenomena in the sea. *Nature* **248,** 394–395 (1974).
5. Komori, S., Murakami, Y. & Ueda, H. The relationship between surface renewal and bursting motions in an open channel flow. *J. Fluid Mech.* **203,** 103–123 (1989).
6. Kumar, S., Gupta, R. & Banerjee, S. An experimental investigation of the characteristics of free-surface turbulence in channel flow. *Phys. Fluids* **10,** 437–456 (1998).
7. Tsai, W. T. A numerical study of the evolution and structure of a turbulent shear layer under a free surface. *J. Fluid Mech.* **354,** 239–276 (1998).
8. Kawanisi, K. & Yokosi, S. Mean and turbulence characteristics in a tidal river. *Estuar. Coast. Shelf Sci.* **38,** 447–469 (1994).
9. Thorpe, S. A. & Hall, A. J. The characteristics of breaking waves, bubble clouds, and near-surface currents using side-scan sonar. *Continent. Shelf Res.* **1,** 353–384 (1983).
10. Belloul, M. B. & Thorpe, S. A. Acoustic observation of oil slicks at sea. *J. Geophys. Res.* **97,** 5215–5220 (1992).
11. Farmer, D. M. & Li, M. Patterns of bubble clouds organized by Langmuir circulation. *J. Phys. Oceanogr.* **25,** 1426–1440 (1995).
12. Thorpe, S. A., Cure, M. S., Graham, A. & Hall, A. J. Sonar observations of Langmuir circulation and estimation of dispersion of floating particles. *J. Atmos. Ocean. Technol.* **11,** 1273–1294 (1994).
13. Thorpe, S. A., Ulloa, M. J., Baldwin, D. & Hall, A. J. An autonomously recording inverted echo sounder; ARIES II. *J. Atmos. Ocean. Technol.* **15,** 1346–1360 (1998).
14. Simpson, J. H. The shelf-sea fronts: implications of their existence and behaviour. *Phil. Trans. R. Soc. Lond. A* **302,** 531–546 (1981).
15. Graham, A. & Hall, A. J. The horizontal distribution of bubbles in a shallow sea. *Continent. Shelf Res.* **17,** 1051–1082 (1997).
16. Thorpe, S. A. On the clouds of bubbles formed by breaking wind-waves in deep water, and their role in air-sea gas transfer. *Phil. Trans. R. Soc. Lond. A* **304,** 155–210 (1982).
17. Stommel, H. Trajectories of small bodies sinking slowly through convection cells. *J. Mar. Res.* **8,** 24–29 (1949).
18. Thorpe, S. A. The effect of Langmuir circulation on the distribution of submerged bubbles caused by breaking wind waves. *J. Fluid Mech.* **142,** 151–170 (1984).
19. Jackson, R. G. Sedimentological and fluid dynamic implications of the turbulent bursting phenomenon in geophysical flows. *J. Fluid Mech.* **77,** 531–560 (1976).
20. Longuet-Higgins, M. S. Surface manifestations of turbulent flow. *J. Fluid Mech.* **308,** 15–29 (1996).
21. Hunt, J. C. R. & Graham, J. M. R. Free stream turbulence near plane boundaries. *J. Fluid Mech.* **84,** 209–235 (1978).
22. Banerjee, S. Upwellings, downdrafts, and whirlpools: dominant structures in free surface turbulence. *Appl. Mech. Rev.* **47,** S166–S172 (1994).
23. Schröder, M. & Siedler, G. Turbulent momentum and salt transport in the mixing zone of the Elbe Estuary. *Estuar. Coast. Shelf Sci.* **28,** 615–638 (1989).
24. Baumert, H. & Radach, G. Hysteresis of turbulent kinetic energy in nonrotational tidal flows: a model study. *J. Geophys. Res.* **97,** 3669–3677 (1992).
25. Bowden, K. F. Horizontal mixing in the sea due to a shearing current. *J. Fluid Mech.* **21,** 83–95 (1965).
26. Fischer, H. B. Longitudinal dispersion and turbulent mixing in open channel flow. *Annu. Rev. Fluid Mech.* **5,** 59–78 (1973).
27. Nimmo Smith, W. A. M. & Thorpe, S. A. Dispersion of buoyant material by Langmuir circulation and a tidal current. *Mar. Pollut. Bull.* (in the press).

28. Ridderinkhof, H. & Zimmerman, J. T. F. Chaotic stirring in a tidal system. *Science* **258,** 1107–1111 (1992).
29. Woolf, D. K. & Thorpe, S. A. Bubbles and the air-sea exchange of gases in near-saturation conditions. *J. Mar. Res.* **49,** 435–466 (1991).

Acknowledgements. We thank T. Lunnel (AEA Tech. plc) for providing the video of the oil slick and the environmental data for the CASI images. We also thank the Environment Agency for supplying the CASI images, and V. Byfield for calibrating them; and A. Hall for help in collecting the sonar data. The observations in the North Sea were funded by an EEC MAST contract. W.A.M.N.S. is supported by NERC.

Correspondence and requests for materials should be addressed to W.A.M.N.S. (e-mail: amns@soc.soton.ac.uk)

Predation enhances complexity in the evolution of electric fish signals

Philip K. Stoddard

Department of Biological Science, Florida International University, Miami, Florida 33199, USA

Theories of sexual selection assume that predation is a restrictive, simplifying force in the evolution of animal display characters[1] and many empirical studies have shown that predation opposes excessive elaboration of sexually selected traits[2]. In an unexpected turnaround, I show here that predation pressure on neotropical, weakly electric fish (order Gymnotiformes) seems to have selected for greater signal complexity, by favouring characters that have enabled further signal elaboration by sexual selection. Most gymnotiform fish demonstrate adaptations that lower detectability of their electrolocation/communication signals by key predators. A second wave phase added to the ancestral monophasic signal shifts the emitted spectrum above the most sensitive frequencies of electroreceptive predators. By using playback trials with the predatory electric eel (*Electrophorus electricus*), I show that these biphasic signals are less detectable than the primitive monophasic signals. But sexually mature males of many species in the family Hypopomidae extend the duration of the second phase of their electric signal pulses[3] and further amplify this sexual dimorphism nightly during the peak hours of reproduction[4]. Thus a signal element that evolved for crypsis has itself been modified by sexual selection.

Weakly electric fish generate multipurpose electric signals for electrolocation and communication[5,6]. Anatomical, physiological and developmental evidence together indicate that the ancestral waveform of the electric organ discharge (EOD) was an intermittent monophasic pulse[5,7–9]. This primitive discharge type is rare in extant gymnotiform fish, having been replaced largely by continuous wave trains (in three families) or multiphasic pulsed waveforms (in three families) (Fig. 1). To address the forces that mould signal complexity, I focus here on the diverse EOD waveforms of pulse-discharging fish. I consider electrolocation, sexual selection and avoidance of predation as possible factors that could favour the switch from a monophasic to a multiphasic EOD.

In fact, electrolocation can favour increased complexity of the EOD, and may well have done so in those species with accessory electric organs and enhanced waveform complexity at the head instead of the tail[9]. But in the biphasic *Brachyhypopomus* species, local biphasy occurs at the tail but not at the head (Fig. 2) where electrosensory exploratory behaviour occurs (P.K.S., unpublished data) and where electroreceptors are most dense[10]. Therefore, among the *Brachyhypopomus* species with biphasic waveforms, the simplest example of signal enhancement, electrolocation could not have been involved with the transition from monophasy to biphasy in the main electric organ.

Most *Brachyhypopomus* species display sexual dimorphism in the second phase of their biphasic pulse EODs, particularly at the tail (Fig. 2)[11–13]. But, before modification for sex recognition and mate attraction[13,14], the second phase would have existed probably in some sexually monomorphic form. Furthermore, in other gymnotiform families—such as Gymnotidae, Rhamphichthyidae and Apteronotidae—this additional phase is present but not sexually dimorphic. Sexual selection thus does support the ancestral conversions from monophasy to biphasy.

Key predators of weakly electric gymnotiforms are pimelodid catfishes and the electric eel[12,15]. Both the Gymnotiformes and their sister order Siluriformes (catfish) possess ampullary electroreceptors with extreme sensitivity to low frequencies[16–18]. The ampullary system is specialized for detecting weak electric fields of prey (passive electrolocation) but is tuned below the spectrum of most gymnotiform EODs. The best frequencies for gymnotiform and catfish ampullary receptors are about 30 Hz and 8 Hz (refs 16, 18) respectively, whereas the spectral peaks of gymnotiform EODs are generally much higher, in the range of 50–3,000 Hz (ref. 19). Gymnotiforms, but not catfish, evolved a second parallel electroreceptive pathway, the tuberous electroreceptor system, two

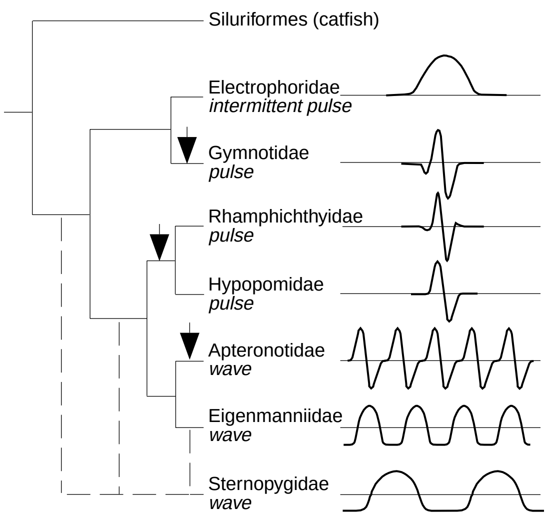

Figure 1 Molecular-morphological consensus phylogeny of the gymnotiform families[22,30] is plotted along with schematic electric organ discharge (EOD) waveforms of representative species. Arrows depict postulated transitions from simple monophasic to multiphasic EOD waveforms. Dashed lines represent equally supported alternate phylogenies. Apteronotidae possess independently derived electric organs, thus the biphasic EOD is derived in this family.

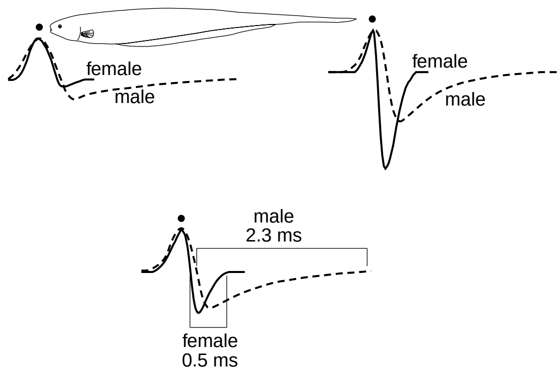

Figure 2 Local and remote EODs of male and female *Brachyhypopomus pinnicaudatus*. EOD waveforms were recorded at locations indicated by the dots. Amplitudes are rescaled here to normalize peaks of the first EOD phase. Note that the EODs are sexually dimorphic, with the male's second phase extended in duration, and that the EOD local to the head is nearly monophasic, particularly in the female.